# Sponge-like molecular cage for purification of fullerenes

Cristina García-Simón, Marc Garcia-Borràs, Laura Gómez, Teodor Parella, Sílvia Osuna, Jordi Juanhuix, Inhar Imaz, Daniel Maspoch, Miquel Costas & Xavi Ribas

## Abstract

Since fullerenes are available in macroscopic quantities from fullerene soot, large efforts have been geared toward designing efficient strategies to obtain highly pure fullerenes, which can be subsequently applied in multiple research fields. Here we present a supramolecular nanocage synthesized by metal-directed self-assembly, which encapsulates fullerenes of different sizes. Direct experimental evidence is provided for the 1:1 encapsulation of C60, C70, C76, C78 and C84, and solid state structures for the host–guest adducts with C60 and C70 have been obtained using X-ray synchrotron radiation. Furthermore, we design a washing-based strategy to exclusively extract pure C60 from a solid sample of cage charged with a mixture of fullerenes. These results showcase an attractive methodology to selectively extract C60 from fullerene mixtures, providing a platform to design tuned cages for selective extraction of higher fullerenes. The solid-phase fullerene encapsulation and liberation represent a twist in host–guest chemistry for molecular nanocage structures.

## Introduction

Fullerenes have a wide range of applications, highlighting their extensive use as electroactive materials in solar cells1,2,3, and with continuously appearing new uses in medicine4,5. Any application, however, is limited in origin by tedious solid–liquid extractions (usually in toluene) and time-expensive chromatographic separations6,7,8,9,10,11,12,13,14,15. More recently, the host–guest chemistry of molecular containers has been explored to encapsulate fullerenes16. Still selectivity is usually difficult to achieve because fine modulation of the size of molecular cages to accommodate different fullerenes is challenging with the limitations of covalent synthesis17. Host platforms containing extended π-systems have been designed because of their affinity towards the sphere-like unsaturated structure of fullerenes. In this line, several covalent or supramolecular approaches pursued include: (a) macrocyclic arene-based receptors18,19,20,21,22,23,24, (b) macrocyclic structures containing aromatic heterocycles25,26,27,28, (c) π-extended TTF receptors29,30,31,32,33 and (d) macrocyclic or jaw-like structures containing porphyrin moieties17,34,35,36,37,38,39,40,41,42,43,44,45. Interestingly, Fujita and co-workers reported the use of the empty channels of a metal–organic framework (MOF) for encapsulating fullerenes upon soaking MOF crystals in fullerene-containing toluene. This work is remarkable because it explores the ability of a solid crystalline structure to absorb fullerenes into its large pores by displacing solvent molecules46.

On the other hand, focusing the interest on selective recovery of encapsulated fullerenes, several strategies have been applied to release the guest molecules as detailed in Fig. 1 (refs 17, 28, 39, 45,

47, 48, 49, 50). In all reported examples, however, there is the need to expose the host to chemical or physical treatment to release the sequestered guests, which prevent its straightforward reusability either because it is blocked by a high-affinity secondary guest, or because the host cage is disassembled. In the case of Fujita's crystalline sponge strategy46, the retention capability is high and half lives of inclusion complexes are over 15 days, thus release of fullerenes must be achieved by deconstructing MOF crystals by acid treatment.

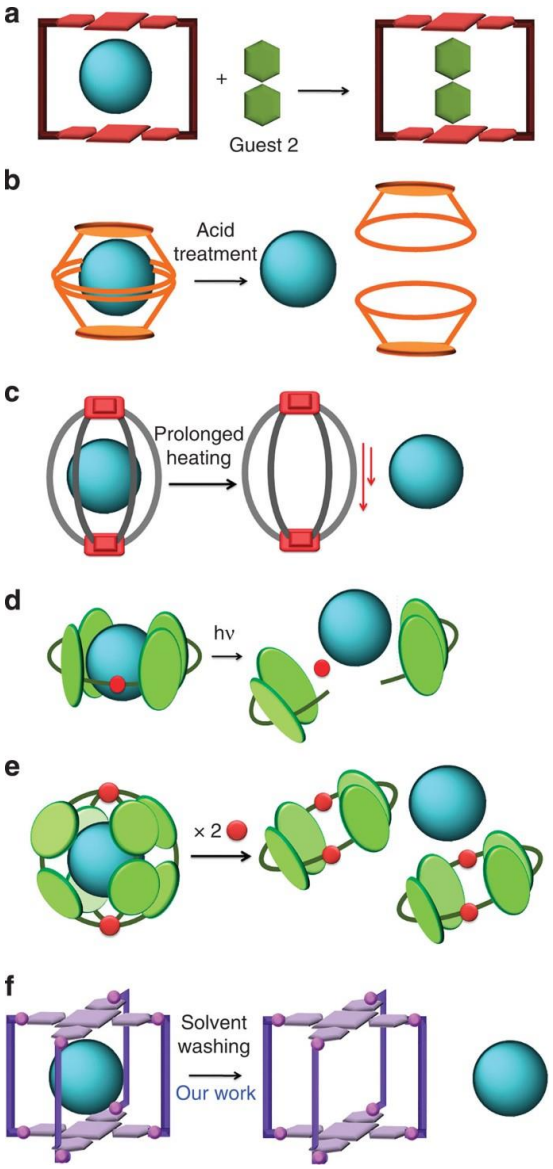


Figure 1: Literature precedents for fullerene liberation from fullerene⊂host adducts. (a) Addition of secondary guests in a guest-exchange process17,39,47, (b) acid or base treatment to provoke a structural rearrangement of the host28, (c) prolonged heating to cause the precipitation of the host48, (d) photoreduction of metal ions to disassemble metal-coordination-based supramolecular hosts49, (e) by transforming the shape of the cage in response to an external stimulus50 and (f) solid–liquid solvent washing strategy.

Here we present a tetragonal prismatic supramolecular cage with a high affinity for the inclusion of fullerenes and a facile ability to release them by solvent washing of the solid inclusion compound. The cage, built by metal-directed self-assembly of two zinc porphyrin moieties and four molecular clips

through Pd coordination bonds, encapsulates exclusively from C60 to C84 fullerenes, and C60 can be selectively released due to their different host affinities. Moreover, the tetragonal prismatic cage design endows four large entrances that enable an unprecedented example of inclusion and release of fullerenes within a molecular cage in the solid state, thus showing a sponge-like behaviour that allows for rapid purification of fullerene mixtures.

## Results

*Synthesis and characterization of 4·(X)8 cages (X=CF3SO3 or BArF (BArF=tetrakis[3,5-bis(trifluoromethyl)phenyl]borate))*

Three-dimensional tetragonal prismatic molecular cage 4·(X)8 was synthesized by self assembly of a tetracarboxylate ZnII-porphyrin and PdII-based macrocyclic synthons ((Pd-1b)·(AcO)2(CF3SO3)2). 4·(X)8 differs from the recently described cage 3·(X')8 (X'=ClO4, CF3SO3) (ref. 51) in the aromatic part of the hexaaza macrocyclic ligands; 3·(X')8 contained 1,4-substituted benzene rings that have been replaced by biphenyl rings in 1b. As a result, the distance between metalloporphyrins is enlarged from 7.5 Å in 3·(X')8 to 14.1 Å in 4·(X)8 (Figs 2 and 3).

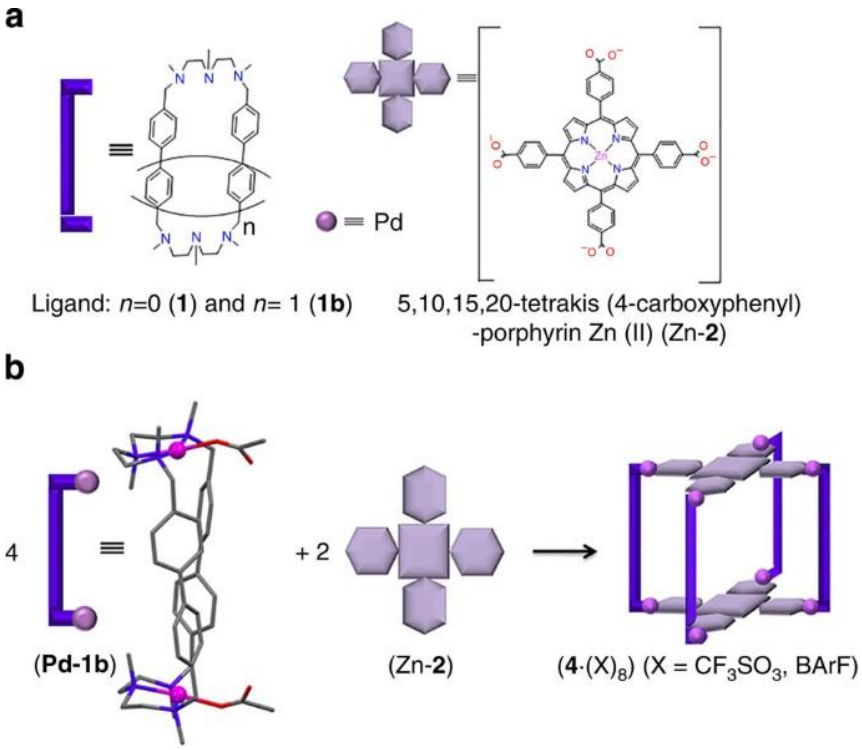


Figure 2: Building blocks to obtain the tetragonal prismatic nanocage 4·(X)8. (a) Building blocks used for (b) the self assembly of molecular clip Pd-1b and tetracarboxylated Zn-porphyrin (Zn-2) to form supramolecular nanocages 4·(X)8 (X=CF3SO3, BArF), (X-ray diffraction of Pd-1b shows one acetate anion coordinated to each Pd centre, and omits the two triflate counteranions for clarity).

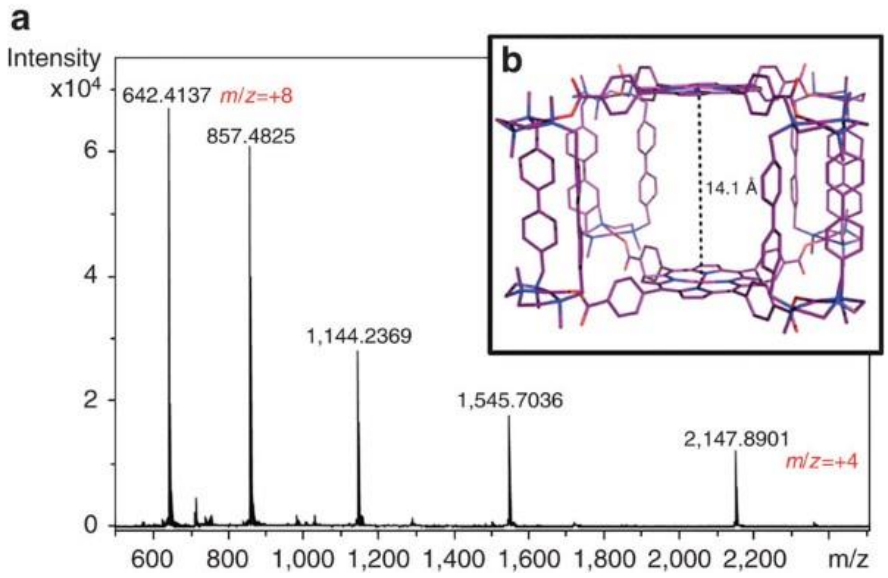


Figure 3: Characterization of 4·(BArF)8. (a) HRMS of 4·(BArF)8. (b) Representation of 48+ extracted from X-ray diffraction data.

Cage 4·(CF3SO3)8 was characterized in solution by electrospray ionization mass spectrometry (ESI-MS). However, the compound was poorly soluble in organic solvents. Improved solubility was exhibited by 4·(BArF)8, which was isolated in 38% yield after anion exchange. The high resolution mass spectrometry (HRMS) spectrum of 4·(BArF)8 shows ions corresponding to the cage with consecutive loss of counteranions, demonstrating its integrity in solution (Fig. 3a). Furthermore, full NMR characterization was performed for 4·(BArF)8, showing that it has a D4h symmetric structure in solution. Importantly, the diffusion-ordered spectroscopy nuclear magnetic resonance (DOSY NMR) experiment afforded a diffusion coefficient of D=3.1 × 10−10 m2 s−1, indicating that the dimensions of 48+ correspond to a hydrodynamic radius of 19.0 Å in solution, in line with the value estimated from crystallographic data (17.4 Å; see Supplementary Table 1). The dimensions of 48+ derived from DOSY NMR are, as expected, larger than in tetragonal cage 38+ (ref. 51).

Crystallographic data were obtained from 4·(BArF)8 crystals at the XALOC beamline of the ALBA Synchrotron (Fig. 3b)52 using MD2M single-axis diffractometer (Maatel, France) and a Pilatus 6 M detector (Dectris, Switzerland). Due to its sensitivity to solvent loss, a crystal of 4·(BArF)8 was measured mounted in a thin glass capillary suspended in ether/dimethylformamide (DMF) (solution used to grow the crystal saturated with ether) and cryopreserved at 100 K. The crystal showed poor diffraction data with reflections of moderate intensity which were further degraded rapidly after 266 degrees oscillation (equivalent to 200 s of collection). This poor density and fast degradation (seen in all measured crystals, including both nanocages 48+ with encapsulated C60 and C70 -vide infra-) could be attributed to the high symmetry, solvent loss and severe motions of the solvents (volatile diethyl ether) and counteranions BArF− molecules in the large cavities of the crystal lattice (see additional comments to X-ray diffraction data in the Supplementary Discussion). All these reasons hampered a complete X-ray diffraction characterization, as counteranions could not be detected and located. Flash cooling the crystals at 100 K by mounting them in a capillary with cryoprotectants did not provide

better crystallographic data. However, the correct structural solution for the cationic molecular cage 48+ was achieved. As expected, nanocage 48+ consists of two parallel tetracarboxylated ZnII-porphyrins (distance between ZnII centres at the porphyrin moieties=14.1 Å) linked by four macrocyclic dinuclear PdII complexes. The four-carboxylate residues of each porphyrin are linked by means of η1-O monodentate coordination to one PdII centre. Altogether, the overall structure is defined as a tetragonal prismatic cage taking the set of eight equivalent atoms of the carboxyphenyl moieties as vertices of the polyhedron, thus bearing D4h symmetry.

*Fullerene encapsulation*

The large void volume of the cage (approximately able to encapsulate a spherical guest of up to 696 Å3) and the known affinity of zinc-porphyrins for fullerenes17, prompted us to explore the capability of 4·(BArF)8 to act as a host for fullerenes. Fast inclusion of C60 occurred during the mixing of a solution of 4·(BArF)8 in acetonitrile with C60 in toluene in a 1:1 molar ratio (Fig. 4). Job plot analysis of ultraviolet–visible (UV–vis) titration data indicated the formation of a 1:1 adduct C60⊂4·(BArF)8 with a high association constant of Ka=2.8 (±0.6)·107 M−1 (logKa=7.44±0.1). The association constant was further confirmed by fluorescence titrations (logKa (fluorescence)=7.47±0.03) (see Supplementary Fig. 1). In addition, a HRMS of this mixture showed exclusively the peaks corresponding to C60⊂4·(BArF)8. Crystals were grown by diethyl ether diffusion over a toluene/acetonitrile (4/1) solution of C60⊂4·(BArF)8 (isolated yield=70%). The 1H-NMR spectra in CD3CN revealed that several aromatic C–H signals had shifted from the spectrum of the empty cage, indicating the inclusion of fullerene in the cage. DOSY NMR experiments afforded a similar hydrodynamic radius for C60⊂4·(BArF)8 when compared with that of the empty cage (see Supplementary Table 1), demonstrating that the molecular entity had not changed in size upon addition of the fullerene. Crystals of C60⊂4·(BArF)8 were also found to be extremely sensitive to solvent loss, therefore we resorted to low temperature X-ray diffraction analysis at the same synchrotron beamline in thin glass capillaries (flash cooling the crystals at 100 K by mounting them in a capillary with cryoprotectants did not afford better diffraction data). As was the case with 4·(BArF)8, a consistent crystallographic solution of the cationic molecular cage was achieved. The studies showed the presence of a spherical electron density at the centre of the cage that fitted nicely to a disordered entrapped C60 molecule (Fig. 4). Detection of this C60 molecule compared with the failure to locate counteranions and solvent guest molecules can be tentatively attributed to its lower mobility inside the cage. Moreover, the computed structure of the host–guest complex C60⊂4·(Cl)8 using state-of-the-art DFT methods showed nice agreement with crystallographic data (Fig. 4; all atoms were calculated at density functional theory (DFT) level). DFT calculations indicated that different orientations of C60 inside the host are accessible (see Supplementary Table 2), thus accounting for the disordered fullerene molecule found in the crystallographic structure.

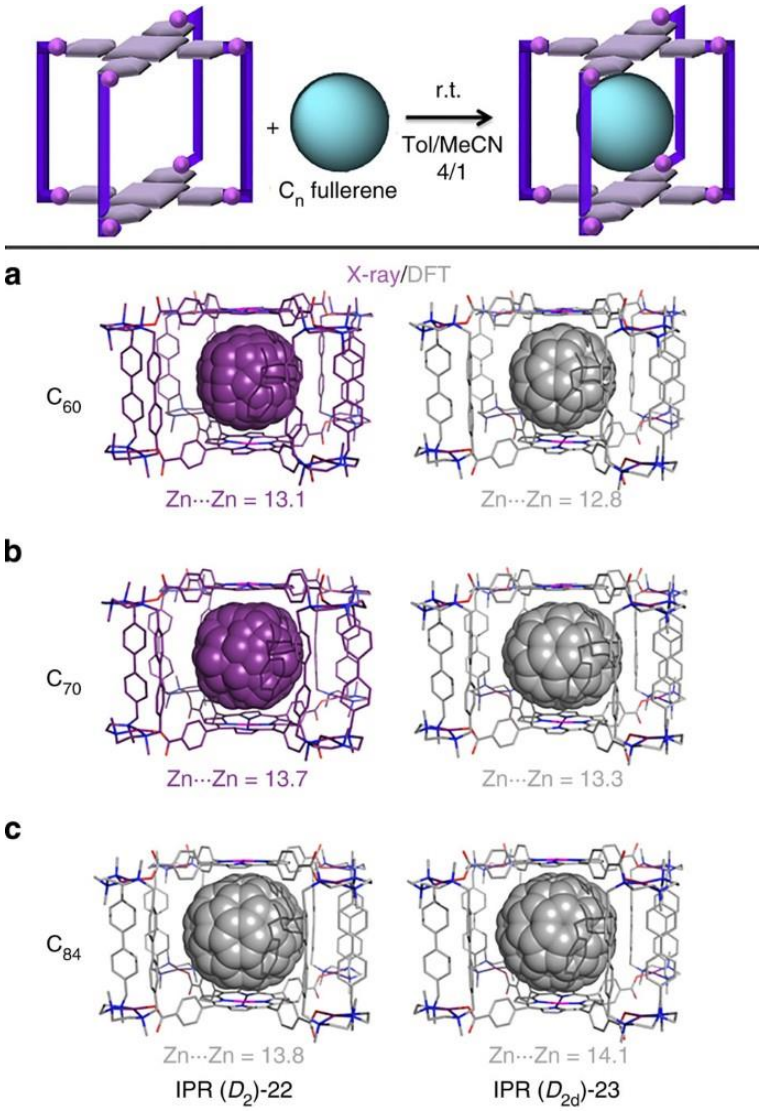


Figure 4: X-ray diffraction and DFT analysis of fullerene host–guest compounds. Crystallographic data (purple) and DFT structures (grey) for cationic fullerene inclusion compounds (a) C60⊂48+ and (b) C70⊂48+; and (c) DFT calculation for C84⊂48+ isomers IPR (D2)-22 and IPR (D2d)-23 (Zn···Zn distances in Å). r.t., room temperature.

We then explored the encapsulation of C70 with 4·(BArF)8 following an equivalent procedure as for C60 (Fig. 4). C70⊂4·(BArF)8 was instantaneously obtained upon mixing host and guest in a 1:1 ratio. UV–vis titration, 1H-NMR and HRMS showed a very favourable association and stability of the inclusion complex in solution. Due to the high affinity of the cage towards the C70, we were unable to obtain an association constant using UV–vis titrations; we therefore resorted to flurorescence titrations and we obtained logKa=8.6±0.3 M−1 (see Supplementary Fig. 2), which is roughly 10-fold higher than for C60. DOSY NMR spectrum also indicated the same diffusion coefficient as for C60⊂4·(BArF)8 and 4·(BArF)8, thus suggesting that C70 is also occupying the inner space of the cage with no substantial volume modification of the whole cage. Crystals were grown by diethyl ether diffusion and measured under synchrotron radiation. Similar problems of location of counteranions and rapid loss of crystallinity were encountered, but yet the data collected allowed identifying the structure of the cationic molecular cage including an ellipsoid-shaped electron density at the centre

of the cage that fits nicely to a disordered C70 molecule, finding the semi-major axis parallel to the porphyrin planes (Fig. 4). DFT calculations indeed indicate that this arrangement is ~6 kcal·mol−1 more stable than the perpendicular alignment. As observed in the case of C60, different orientations of the C70 molecule with the semi-major axis parallel to the porphyrin planes are accessible, thus indicating that the fullerene moiety can easily rotate (see Supplementary Table 3). The DFT-optimized C70⊂4·(Cl)8 structure also showed nice agreement with crystallographic data (Fig. 4; all atoms were calculated at DFT level).

Comparison of crystallographic data for 4·(BArF)8, C60⊂4·(BArF)8 and C70⊂4·(BArF)8 shows that porphyrin–porphyrin interdistance is maximized (14.1 Å) when guest molecule is absent, whereas the inclusion of C70 compressed this distance down to 13.7 Å and inclusion of C60 further shrinks it to 13.1 Å (Table 1). DFT-optimized structures are in line with the observed experimental trends. Therefore, the sum of structural and computational information shows an important degree of adaptability or 'breathing' of the cage by maximizing the porphyrin–fullerene interaction (see Supplementary Fig. 3).

| | | Crystallographic data | DFT data |
|---|---|---|---|
| $C_{60}⊂\mathbf{4}^{8+}$ | Zn···Zn (in Å) | 13.1 | 12.8 |
| | C20-C20′-C20′′-C45 (torsion angle (°)) | −175.7 | −173.5 |
| $C_{70}⊂\mathbf{4}^{8+}$ | Zn···Zn | 13.7 | 13.3 |
| | C20-C20′-C20′′-C45 | −176.3 | −175.7 |
| $C_{84}⊂\mathbf{4}^{8+}$ | Zn···Zn | — | 13.8 |
| ($(D_2)$-22) | C20-C20′-C20′′-C45 | — | −177.0 |
| $C_{84}⊂\mathbf{4}^{8+}$ | Zn···Zn | — | 14.1 |
| ($(D_{2d})$-23) | C20-C20′-C20′′-C45 | — | −177.6 |
| $\mathbf{4}^{8+}$ | Zn···Zn | 14.1 | 11.8 |
| | C20-C20′-C20′′-C45 | −178.9 | −169.4 |

Table 1 Structural data. DFT, density functional theory. Relevant experimental and theoretical structural data for C60⊂48+, C70⊂48+, C84⊂48+ and 48+ (see Supplementary Fig. 6 for details on the torsion angle measurement).

Given the large void space of the cage 4·(BArF)8, we explored the limits of encapsulation of higher fullerenes and chemically modified fullerenes. To that end, we selected the larger C84 and [60]PCBM ([6,6]-phenyl-C61-butyric acid methyl ester). Both of them were encapsulated in a 1:1 fashion forming C84⊂4·(BArF)8 and [60]PCBM⊂4·(BArF)8, as indicated by HRMS. The extremely low solubility of C84 precluded NMR and UV–vis host–guest studies. On the other hand, HRMS for [60]PCBM⊂4·(BArF)8 also indicated a clean 1:1 adduct and did not show desymmetrization of the 1H-NMR signals, suggesting that the inner space is large enough to allow free rotation of the anisotropic [60]PCBM. Moreover, model C84⊂4·(Cl)8 species were optimized at a DFT level, selecting the two most abundant isomers ((D2)-22 and (D2d)-23 IPR (Isolated-Pentagon-Rule) isomers, see Fig. 4 and Supplementary Figs 4 and 5). The computational investigation of C84 encapsulation inside the host indicated that the porphyrin–porphyrin interdistance is elongated ~0.5 Å with respect to C70⊂4·(Cl)8. This value is similar to the porphyrin–porphyrin distance found for the empty nanostructure, indicating that there exists a good fit between C84 and the cavity of the host cage. 4·(BArF)8 is thus capable of unusually facile encapsulation of C60, C70, C84 and [60]PCBM.

Relative affinity for the most abundant and accessible C60 with respect to C70 was also explored in a HRMS study; one equivalent of 4·(BArF)8 was mixed with one equivalent of C60 and one equivalent of C70 in a 4:1 toluene:acetonitrile solvent mixture. HRMS of the resulting solution showed a preferential encapsulation of C70 with a 9:1 peak intensity ratio for C70⊂4·(BArF)8 versus C60⊂4·(BArF)8. On the other hand, when one equivalent of 4·(BArF)8 is combined with 10 equivalents of C60 and one equivalent of C70, two equally intense signals are found for C60⊂4·(BArF)8 and C70⊂4·(BArF)8. Finally, a mixture of one equivalent of 4·(BArF)8 with one equivalent of C60 and nine equivalents of C70 completely excludes the noticeable encapsulation of C60 and C70⊂4·(BArF)8 is exclusively observed by HRMS. Substoichiometric additions of C60 and C70 confirmed the same MS ionization behaviour of free host, host-C60 and host-C70 compounds, meaning that the relative intensity of the peaks corresponding to host-C60 and host-C70 with the same charge reproduce their relative concentration in solution. An estimation of the affinity to the host for the two fullerenes could then be extracted from this analysis, revealing that C70 bears a nine-fold higher affinity for 4·(BArF)8 than C60, in agreement with the 10-fold difference in association constants found by fluorescence spectroscopy studies. These results are rationalized by a higher degree of π-interactions with C70 due to its ellipsoid shape (see Supplementary Figs 7–10). This is confirmed by DFT calculations, which indicate a more favourable porphyrin–fullerene interaction for C70 fullerene molecule (see Supplementary Fig. 11 and Supplementary Tables 3 and 4). These results are consistent with the X-ray diffraction data in which C70⊂4·(BArF)8 presents a less-strained cage conformation, closer to its form as empty cage 4·(BArF)8, while the more distorted cage in case of C60⊂4·(BArF)8 gives a less stable adduct.

The inclusion of fullerenes in 4·(BArF)8 is also observed by using fullerene extract (SES Research, C60 70%, C70 28%, higher fullerenes 2%). HRMS of the inclusion compounds formed upon mixing 4·(BArF)8 with fullerene extract (1:3 molar ratio, assuming that all fullerenes are C60) in a mixture of toluene/acetonitrile (4/1) exhibited the ion peaks corresponding to C60⊂4·(BArF)8, C70⊂4·(BArF)8 and C84⊂4·(BArF)8 as the main signals, although minor ion peaks corresponding to C76⊂4·(BArF)8 and C78⊂4·(BArF)8 were also observed. The C60⊂4/C70⊂4 and C70⊂4/C84⊂4 ratios derived from the relative intensity of the ion peaks are 0.72 and 12.8, respectively. However, when using different excesses of fullerene, enrichment of the proportion of higher fullerenes caged was observed. Thus, for 1:12 cage:fullerene extract molar ratios, mass spectra affords C60⊂4/C70⊂4 and C70⊂4/C84⊂4 ratios of 0.18 and 11.3, respectively, whereas larger excess (1:60 weight ratio) afforded C60⊂4/C70⊂4 and C70⊂4/C84⊂4 ratios of 0.05 and 6.7, respectively (see Supplementary Fig. 12). Therefore, the initial 30% content of C70 and higher fullerenes is remarkably improved to >96% after a single extraction with 4·(BArF)8.

On the other hand, when fullerene soot (Aldrich, C60 5.3%, C70 1.54%, higher fullerenes 0.14%, the rest being other forms of carbon) is suspended in toluene and reacted with 4·(BArF)8 (1:12 cage:soot weight ratio; final solvent mixture toluene/acetonitrile 4/1), similar ratios of encapsulation as for fullerene extract were found (see Supplementary Fig. 13).

The versatility of the cage is further exemplified by the fact that encapsulation of fullerenes can be performed by soaking 4·(BArF)8 as a solid (grain size: 3.1±3.0 μm; median: 2.2 μm; Supplementary Fig. 14)53 in a C70-containing toluene solution, thus being the first example of solid-phase fullerene

encapsulation for a supramolecular cage (to our knowledge, a single similar precedent using a MOF was reported by Fujita and co-workers)46. This observation discards partial cage disassembly during the host–guest event, and agrees with a guest encapsulation occurring by fullerene entrance through the four apertures of the cage; the dimensions of the apertures are large enough to envision the mobility of fullerene molecules through them. Moreover, we could also modify the selectivity toward higher fullerenes, using solid 4·(BArF)8 and fullerene extract dissolved in toluene by changing the fullerene extract ratio used (see Supplementary Figs 15–16). These results prompted us to investigate the encapsulation of C70 dissolved in toluene and insoluble 4·(CF3SO3)8 as solvent-evacuated crystals. After 5–10 min, complete inclusion was obtained forming C70⊂4·(CF3SO3)8, as ascertained by HRMS (Supplementary Fig. 17).

## Discussion

Once the inclusion of fullerenes (from C60 to C84) was thoroughly studied, we sought to find a straightforward experimental protocol to liberate the different fullerenes in a selective manner. Taking advantage of the fact that fullerenes are encapsulated in the solid state, we charged solid 4·(BArF)8 nanocapsule (0.33 µmols) together with Celite in a short column. Subsequently, a 1.4 mM solution of C60 was passed through the column seven times, and total encapsulation was confirmed by HRMS. Afterwards, the extraction of C60 from the solid sample of C60⊂4·(BArF)8 charged in the column was performed by consecutive washings with 1,2-dichlorobenzene/CS2 (1/1 v/v mixture). This solvent mixture fulfills the requirements of a very high solubility of fullerenes and very low solubility of either C60⊂4·(BArF)8 or 4·(BArF)8. We were delighted to observe that washing with 5 × 1 ml of the 1,2-dichlorobenzene/CS2 mixture was sufficient to liberate all encapsulated C60 (see Fig. 1f). On the other hand, the solid remaining in the filtration column was found to be 4·(BArF)8, which was ready to be filled again with C60. The solid fullerene encapsulation–extraction protocol was repeated up to five cycles (see flow chart in Supplementary Fig. 18). After these cycles, 91% of 4·(BArF)8 was recovered from the column by washing with acetonitrile (Fig. 5a). To the best of our knowledge, this is the first example of the use of orthogonal solubility of the host and fullerene for the extraction of fullerenes (only the reverse adsorption of fullerenes by soaking a MOF crystal in fullerene-containing toluene was reported by Fujita and co-workers)46.

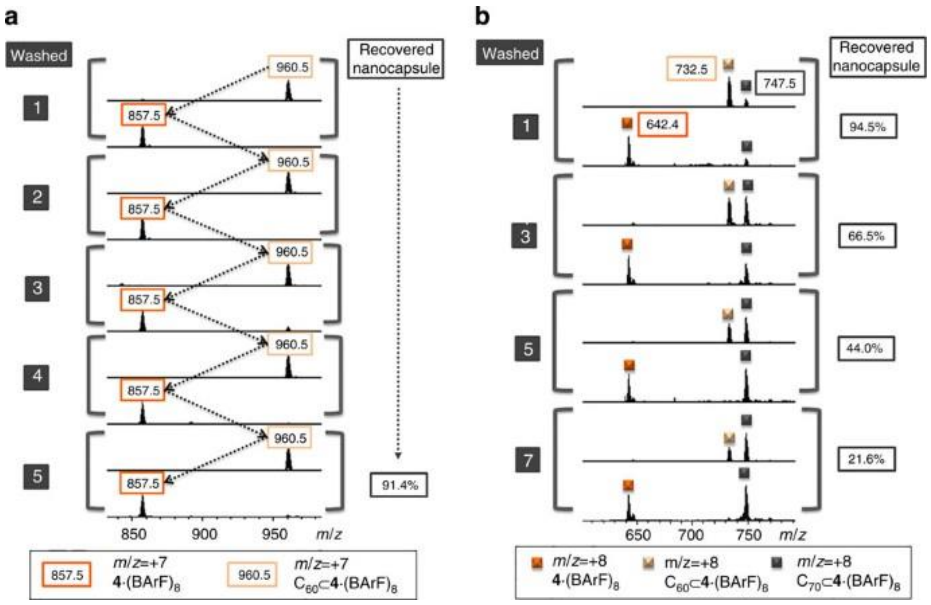

Figure 5: Solid state extraction of fullerenes from 4·(BArF)8. HRMS monitoring of the C60 extraction washing-protocol using (a) pure C60 encapsulated in 4·(BArF)8 in the solid phase and (b) fullerene extract encapsulated in 4·(BArF)8.

The same protocol was attempted for the inclusion of a mixture of fullerenes (fullerene extract). However, ineffective mixing at the column between the solid 4·(BArF)8 and the toluene solution containing fullerene extract afforded inhomogeneous distribution of fullerenes among the solid. We therefore decided to improve the encapsulation step by re-dissolving the empty cage in CH3CN and performing the encapsulation of fullerene extract in solution (1:1 molar ratio). Subsequently, the fullerene-containing cage was precipitated out by the addition of diethyl ether and the filled cage reintroduced in the column (see Supplementary Fig. 19). At the first cycle, C60⊂4/C70⊂4 ratio was 4.0 (by HRMS), and only C60 was released after washing the solid inclusion compound with 1,2-dichlorobenzene/CS2 (1/1 v/v mixture). After repeating the inclusion and liberation sequence up to seven cycles (Fig. 5b), the cage was enriched with C70 at each cycle and was finally saturated of mainly C70 and C84 (an ~10% mass loss was observed after each cycle due to the experimental setup). The maximum extraction capacity was calculated as 1 mol of C60 per mol of cage 4·(BArF)8, and a 61% of the expected C60 was recovered (quantified by UV–vis). Overall, this experiment demonstrates that the simple and fast selective C60 purification from a mixture of fullerenes is feasible by using cage 4·(BArF)8 and our solvent-washing protocol54.

Regarding the recovery of higher fullerenes (mainly C70 and C84) trapped in the saturated sample of 4·(BArF)8 after multiple encapsulation/liberation cycles, we tested other solvent mixtures but no significant liberation of higher fullerenes was achieved. Therefore, we resorted to triflic acid (10 equivalents) treatment (in toluene) of C70 and C84⊂4·(BArF)8 in the solid state to disassemble the cage and rapid release of the mixture of higher fullerenes into toluene solution. Further partial reassembly of cage 4·(CF3SO3)8 upon base (NEt3) neutralization and reflux in DMF occurred, as ascertained by HRMS (see Supplementary Fig. 20).

To sum up, we have designed the new molecular cage 4·(BArF)8 that encapsulates fullerenes (from C60 to C84) in a fast manner at room temperature. At the core of the adaptability of the cages to bind substrates that differ substantially in size is the remarkable ability to modulate the size of the cavities by alteration of porphyrin–porphyrin distances. This molecular ‘breathing’ ability of the cages relies on the substantial degree of flexibility of metal-coordination (Pd-carboxylate) bonds in the clips that hold the supramolecular structure. Full spectroscopic and spectrometric characterization of the host and host–guest compounds is reported. In addition, a sponge-like behaviour has been proven for 4·(BArF)8 for the selective purification of C60 from a mixture of fullerenes. This study provides fundamental results regarding the ability of the described tetragonal nanocage to encapsulate and liberate fullerenes, and paves the way to study the performance of newly designed cages (varying the nature of metalloporphyrin moieties, decorating the apertures of the cage, changing Pd cations at the molecular clips by first-row transition metals, and so on) to finely tune the selectivity for higher fullerenes or endohedral fullerenes. Here we demonstrate for the first time that the encapsulation event can occur by soaking the molecular nanocage in the solid state in a fullerene-containing toluene solution. Moreover, the liberation of C60 is also achieved by applying solvent-washing protocols to

the host–guest complex in the solid state. We envision these findings may spark supramolecular host-guest research in the solid phase in cages bearing apertures for guest entrance.

## Methods

*Materials and instrumentation*

Reagents and solvents used were commercially available reagent quality unless indicated otherwise. Ligand H2pp (see Supplementary Fig. 21) was synthesized according to published procedures55. NMR data concerning product identity were collected on Bruker 400 MHz AVANCE spectrometers in CDCl3 or CD3CN, and calibrated relative to the residual protons of the solvent. ESI-MS experiments were collected and analysed on both a Bruker Daltonics Esquire 6000 spectrometer and a Bruker MicroTOF-Q-II, using acetonitrile or DMF as the mobile phase. UV–vis spectroscopy was performed on an Agilent 8452 UV–vis spectrophotometer with 1 cm quartz cell, equipped with a temperature control cryostat from Unisoku Scientific Instruments (Japan), using a toluene/acetonitrile 9/1 (v/v) mixture as solvent. Fluorescence measurements were performed in a Spectrofluorimeter Fluorolog Horiba Jobin Yvon.

*Synthesis and characterization of 1b ligand*

0.66 g of H2pp (1.2 mmols) are added to a 100 ml flask and mixed with: 10 ml of formaldehyde, 8 ml of formic acid and 10 ml of water. The resulting mixture is heated to reflux during 12 h. After this time, the reaction mixture is cooled to room temperature and the solvent removed under reduced pressure. Then 25 ml of NaOH 30% are added. The product is extracted with CHCl3 (3 × 25 ml). Organic phases are combined, dried with anhydrous MgSO4 and filtered. The remaining solution is dried under vacuum, and the obtained product purified by recrystallization with acetone. (Yield: 51.8%). 1H-NMR (400 MHz, CDCl3) δ p.p.m.: 7.39 (d, J=8.24 Hz, 8H, arom), 7.29 (d, J=8.24 Hz, 8H, arom), 3.47 (s, 8H, CH2), 2.57–2.49 (m, 16H, CH2), 2.28 (s, 6H, CH3), 2.22 (s, 12H, CH3). 13C-NMR (75 MHz, CD3CN) δ p.p.m.: 139.5 (arom), 137.9 (arom), 129.5 (arom), 126.7 (arom), 62.3 (–CH2– benzylic), 54.8 (–CH2–), 54.4 (–CH2–), 43.6 (N–CH3), 42.9 (N–CH3). Fourier transform infrared (spectroscopy) ν (cm−1): 1,462 (C–N st), 1,650–2,000, 2,780 (C–H st, sp3), 2,935 (arC–H st), 2,967 (C–H st, sp2). ESI-MS (m/z): calculated 647.9 and found 647.4 ({Me2pp+H}+). For NMR and ESI-MS analysis of 1b, see Supplementary Figs 21–25.

*Synthesis and characterization of 1b·(AcO)2(CF3SO3)2 molecular clip*

In a round-bottom flask, 0.08 g of 1b ligand (0.125 mmols), 0.058 g of Pd(AcO)2 (0.250 mmols) and 25 ml of anhydrous CH3CN were mixed. The mixture is heated to reflux temperature, under nitrogen atmosphere for 18 h. After this time, the reaction mixture is cooled down to room temperature. Subsequently, an excess of NaCF3SO3 salt is added (0.525 mmols) and the mixture is stirred vigorously for 6 h. The reaction mixture is concentrated to a volume of 2–3 ml under reduced pressure, filtered through Celite and recrystallized under slow diethyl ether diffusion. Yellow crystalline solid is obtained. (Yield: 90.1%). 1H-NMR (400 MHz, CD3CN) δ p.p.m.: 8.37 (d, J=8 Hz, 10.5 H, arom), 8.15 (d, J=8 Hz, 8 H, arom), 7.94 (d, J=8 Hz, 2.5 H, arom), 4.06 (d, J=13 Hz, 5.25 H, –CH2–), 3.62 (m, 5.26 H, –CH2–), 3.33 (s, 11.9 H, N–CH3), 3.31 (s, 3.6 H, N–CH3), 3.25 (m, 5.25 H, –CH2-), 3.11 (d, J=13 Hz, 5.17 H, –CH2–), 2.38 (d, J=14 Hz, 5.0 H, –CH2–), 2.30 (d, 5.2 H, –CH2–), 2.07 (s, 5.9 H, AcO), 2.05 (s, 1.8 H, AcO), 1.50 (s, 1.8 H, N–CH3), 1.41 (s, 6.0 H, N–CH3). 13C-NMR (100 MHz, CD3CN) δ p.p.m.: 178.7 (C=O,

AcO), 142.2 (arom), 141.03 (arom), 133.8 (arom), 133.6 (arom), 128.5 (arom), 128.1 (arom), 65.6 (–CH2–), 65.4 (–CH2–), 61.0 (–CH2–), 60.8 (–CH2–), 59.0 (–CH2–), 58.9 (–CH2–), 50.8 (N–CH3), 43.9 (N–CH3), 43.5 (N–CH3), 24.2 (–CH3, AcO), 24.1 (–CH3, AcO). HRMS (m/z): calculated 1,127.259 and found 1,127.257 ({[Pd-1b·(AcO)2](CF3SO3)1}1+), calculated 489.154 and found 489.153 ({[Pd-1b·(AcO)2]}2+). For NMR, IR and ESI-MS analysis of the Pd-1b·(AcO)2(CF3SO3)2 compound, see Supplementary Figs 26–32.

*Synthesis of 4·(BArF)8 molecular cage*

10.56 mg of 5,10,15,20-tetrakis(4-carboxyphenyl)porphyrin-ZnII (2, 0.01 mmols) are weighed in a 10 ml flask, then 1 ml of DMF is added. Then, 10 µl of triethylenetriamine dissolved in 0.5 ml of DMF are added to the porphyrin solution. Finally 30 mg of Pd-1b·(AcO)2(CF3SO3)2 (0.02 mmols) complex dissolved in 2.5 ml of DMF are added to the mixture. The solution obtained is heated to 105 °C under reflux for 16 h. After the reaction time, the mixture is cooled to room temperature, filtered through Celite and recrystallized by diethyl ether diffusion. The 4·(CF3SO3)8 crystalline solid obtained (extremely low solubility prevented NMR characterization; however, high sensibility of HRMS analysis allowed its mass spectrometry characterization, see Supplementary Fig. 33) is suspended in 12 ml of DCM, an excess of NaBArF salt is added (1 to 10 equivalents) and the mixture is stirred vigorously for 16 h. The reaction mixture is filtered. The product is obtained by precipitation with diethyl ether. The purple powder is washed several times with diethyl ether to remove the excess of NaBArF. (Yield: 38.3%). 1H-NMR (400 MHz, CD3CN) δ p.p.m.: 8.60 (dd, 8H, arom-porph), 8.58 (s, 16H, pyrrole ring), 8.35 (dd, J=8 Hz, 8H, arom-porph), 8.30 (d, J=8.5 Hz, 32H, arom-clip), 8.15 (d, J=8.5 Hz, 32H, arom-clip), 8.10 (dd, J=8 Hz, 8H, arom-porph), 7.98 (dd, J=8 Hz, 8H, arom-porph), 7.68 (m, 96H, NaBArF), 4.07 (d, J=13 Hz, 16H, –CH2–), 3.70 (m, 16H, –CH2–), 3.60 (s, 48H, N–CH3), 3.38 (m, 16H, –CH2–), 3.15 (d, J=13 Hz, 16H, –CH2–), 2.49 (dd, J=13.5, 16H, –CH2–), 2.39 (dd, J=13.5, 16H, –CH2–), 1.58 (s, 24H, N–CH3). 13C-NMR (100 MHz, CD3CN) δ p.p.m.: 206.7 (BArF), 166.0 (DMF), 160.4 (BArF), 148.8 (pyrrole ring), 140.4 (arom-clip), 134.6 (BArF), 133.8 (arom-porph), 133.1 (arom-clip), 133.1 (arom-porph), 129.7 (pyrrole ring), 127.1 (arom-clip), 127.1 (arom-porph), 116.6 (BArF), 64.7 (–CH2–), 60.2 (–CH2–), 59.1 (–CH2–), 51.6 (NCH3), 42.6 (NCH3). HRMS (m/z): calculated 2,147.893 and found 2,147.893 ({4·(BArF)4}4+); calculated 1,545.701 and found 1,545.702 ({4·(BArF)3}5+), calculated 1,144.239 and found 1,144.242 ({4·(BArF)2}6+); calculated 857.481 and found 857.483 ({4·(BArF)}7+); calculated 642.413 and found 642.414 ({4·(BArF)}8+). For NMR and HRMS analysis of the 4·(BArF)8 compound, see Supplementary Figs 34–40.

*Preparation and characterization of the fullerene adducts*

Preparation of C60⊂4·(BArF)8: 2.5 mg of 4·(BArF)8 nanocapsule (0.2 µmols, 1 equivalent) were dissolved in 100 µl of CH3CN. Then one equivalent of C60 dissolved in 400 µl of toluene was added to the cage solution. The mixture was stirred at room temperature for 5 min. The mixture is filtered and recrystallized by diethyl ether diffusion. 1H-NMR (400 MHz, CD3CN) δ p.p.m.: 8.64 (dd, 8H, arom-porph), 8.55 (s, 16H, pyrrole ring), 8.35 (dd, J=8 Hz, 8H, arom-porph), 8.30 (d, J=8.5 Hz, 32H, arom-clip), 8.14 (d, J=8.5 Hz, 32H, arom-clip), 8.04 (dd, J=8 Hz, 8H, arom-porph), 7.99 (dd, J=8 Hz, 8H, arom-porph), 7.68 (m, 96H, NaBArF), 4.07 (d, J=13 Hz, 16H, –CH2–), 3.70 (m, 16H, –CH2–), 3.60 (s, 48H, N–CH3), 3.38 (m, 16H, –CH2–), 3.15 (d, J=13 Hz, 16H, –CH2–), 2.49 (dd, J=13.5, 16H, –CH2–), 2.39 (dd, J=13.5, 16H, –CH2–), 1.58 (s, 24H, N–CH3). HRMS (m/z): calculated 2,328.143 and found 2,328.144 ({C60⊂4·(BArF)4}4+); calculated 1,689.901 and found 1,689.902 ({C60⊂4·(BArF)3}5+), calculated

1,264.406 and found 1,264.408 ({C60⊂4·(BArF)2}6+); calculated 960.339 and found 960.341 ({C60⊂4·(BArF)}7+); calculated 732.413 and found 732.415 ({C60⊂4·(BArF)}8+).

Preparation of C70⊂4·(BArF)8: 2.5 mg of 4·(BArF)8 nanocapsule (0.2 µmols, one equivalent) was dissolved in 100 µl of CH3CN. Then one equivalent of C70 dissolved in 400 µl of toluene was added to the cage solution. The mixture was stirred at room temperature for 5 min. The mixture is filtered and recrystallized by diethyl ether diffusion. 1H-NMR (400 MHz, CD3CN) δ p.p.m.: 8.66 (dd, J=8 Hz, 8H, arom-porph), 8.48 (s, 16H, pyrrole ring), 8.33 (dd, 8H, arom-porph), 8.33 (d, J=8.5 Hz, 32H, arom-clip), 8.18 (d, J=8.5 Hz, 32H, arom-clip), 8.00 (m, J=8 Hz, 8H, arom-porph), 7.97 (m, J=8 Hz, 8H, arom-porph), 7.68 (m, 137H, NaBArF), 4.09 (d, J=13 Hz, 16H, –CH2–), 3.70 (m, 16H, –CH2–), 3.60 (s, 48H, N–CH3), 3.38 (m, 16H, –CH2–), 3.15 (d, J=13 Hz, 16H, –CH2–), 2.49 (dd, J=13.5, 16H, –CH2–), 2.39 (dd, J=13.5, 16H, –CH2–), 1.59 (s, 24H, N–CH3). HRMS (m/z): calculated 2,358.143 and found 2,358.141 ({C70⊂4·(BArF)4}4+); calculated 1,713.901 and found 1,713.900 ({C70⊂4·(BArF)3}5+), calculated 1,284.406 and found 1,284.409 ({C70⊂4·(BArF)2}6+); calculated 977.624 and found 977.625 ({C70⊂4·(BArF)}7+); calculated 747.413 and found 747.413 ({C70⊂4·(BArF)}8+).

Preparation of [C60]PCBM⊂4·(BArF)8: 2.5 mg of 4·(BArF)8 nanocapsule (0.2 µmols, one equivalent) were dissolved in 100 µl of CH3CN. Then one equivalent of [C60]PCBM dissolved in 400 µl of toluene was added to the cage solution. The mixture was stirred at room temperature for 5 min. The mixture is filtered and recrystallized by diethyl ether diffusion. 1H-NMR (400 MHz, CD3CN) δ p.p.m.: 8.60 (dd, J=8.0 Hz, 8H, arom-porph), 8.50 (s, 16H, pyrrole ring), 8.35 (dd, J=8.0 Hz, 8H, arom-porph), 8.32 (d, J=8.5 Hz, 32H, arom-clip), 8.13 (d, J=8.5 Hz, 32H, arom-clip), 7.99 (m, J=8 Hz, 8H, arom-porph), 7.92 (m, J=8 Hz, 8H, arom-porph), 142 (m, 96H, NaBArF), 4.09 (d, J=13 Hz, 16H, –CH2–), 3.67 (m, 16H, –CH2–), 3.60 (s, 48H, N–CH3), 3.38 (m, 16H, –CH2–), 3.15 (d, J=13 Hz, 16H, –CH2–), 2.49 (dd, J=13.5, 16H, –CH2–), 2.40 (dd, J=13.5, 16H, –CH2–), 1.59 (s, 24H, N–CH3). HRMS (m/z): calculated 2,375.668 and found 2,375.667 ({[C60]PCBM⊂4·(BArF)4}4+); calculated 1,727.921 and found 1,727.923 ({[C60]PCBM⊂4·(BArF)3}5+), calculated 1,296.089 and found 1,296.088 ({[C60]PCBM⊂4·(BArF)2}6+); calculated 987.639 and found 987.636 ({[C60]PCBM⊂4·(BArF)}7+); calculated 756.175 and found 756.173 ({[C60]PCBM⊂4·(BArF)}8+).

For NMR and HRMS analysis of the host–guest adducts, see Supplementary Figs 41–55.

*General procedures for UV–vis and fluorescence titrations*

Host–guest interactions in solution were studied by UV–vis and fluorescence spectroscopy. The UV–vis titration experiments between 4·(BArF)8 (4.32 × 10−7 M) and the different fullerenes tested (1.39 × 10−5 M) were performed by using toluene/acetonitrile (9/1) as solvent. The cage concentration was kept constant. The C60 (3.46 × 10−6 M) titration was repeated using a constant concentration of 4·(BArF)8 of 1.08 × 10−7 M. A magnetic stir bar and 2 ml of nanocapsule solution were added to the cuvette, then it was inserted into the spectrometer and the stirrer activated and the substrate added. The stoichiometry of the complexes was studied using the method of continuous variations. Solutions of nanocapsule 4·(BArF)8 and fullerenes (4.32 × 10−7 M) in toluene/acetonitrile (9/1) were mixed at different ratios. All the experiments were carried out at 22 °C. The fluorescence titration for C60 was performed under the same conditions of the UV–vis titration. C70 fluorescence titration experiment

was performed using a 1.08 × 10−8 M solution of 4·(BArF)8 and 3.46 × 10−7 M solution of C70. A 9/1 mixture of toluene/acetonitrile was used as solvent and the cage concentration was kept constant.

The data obtained from the UV–vis and the fluorescence spectrophotometric titrations were analysed using the software Origin Pro 8 and SPECFIT 3.0 from Spectrum Software Associates, Marlborough, MA, U.S.A. (SpecSoft@compuserve.com), which uses a global system with expanded factor analysis and Marquardt least-squares minimization to obtain globally optimized parameters. For UV–vis titrations of the host–guest adducts, see Supplementary Figs 56–60.

*Diffusion-ordered NMR spectroscopy experiments*

Diffusion-ordered NMR experiments (DOSY NMR) of Pd-1b·(AcO)2(CF3SO3)2, 4·(BArF)8, C60⊂4·(BArF)8 and C70⊂4·(BArF)8, allow the determination of the translational self-diffusion coefficients (D) for these species in acetonitrile solution. Making use of the Stokes–Einstein equation (equation 1), the hydrodynamic radii (rH) for the diffused species can be calculated from the D value (see obtained values on Supplementary Table 1).

$$D = \frac{\mathrm{k} \cdot T}{6 \cdot \pi \cdot \eta \cdot r_{\mathrm{H}}} \qquad (1)$$

where k is the Boltzmann constant, T is the temperature, and η is the viscosity of the solvent (η (CH3CN)=0.35 mPa s) (ref. 56).

The DOSY spectra were acquired using the LEDBP pulse sequence using 16 transients and eight dummy scans, at 298 K. The diffusion time D was 150 ms and the total diffusion-encoding gradient duration (d) was 1.1 ms. Sixteen values of diffusion-encoding gradient were used, varying from approximately 1 to 50 G cm−1 in equal steps of gradient squared. Data were acquired and processed using the automated ‘dosy’ and ‘dosy2d’ macros incorporated into the TOPSPIN v2.1 software package (Bruker Biospin, Rheinstetten, Germany). For DOSY-NMR experiments of the host–guest adducts, see Supplementary Figs 61–64.

*X-ray diffraction studies details*

Crystallographic data for Pd-1b·(AcO)2(CF3SO3)2 were collected using Bruker-AXS SMART-APEXII CCD diffractometer (MoKα, λ=0.71073 Å). Indexing was performed using APEX2 (Difference Vectors method). Data integration and reduction were performed using SaintPlus 6.01. Absorption correction was performed by multi-scan method implemented in SADABS. The structure was solved using SHELXS-97 and refined using SHELXL-97 contained in SHELXTL program. All hydrogen atoms were placed using a riding model. Their positions were constrained relative to their parent atom using the appropriate HFIX command in SHELXL-97. See Supplementary Data 2.

Crystallographic data for 4·(BArF)8, C60⊂4·(BArF)8 and C70⊂4·(BArF)8 samples were collected at the XALOC beamline of the ALBA synchrotron at 100 K using a MD2M single-axis diffractometer (Maatel, France) and a Pilatus 6 M detector (Dectris, Switzerland). Due to their sensitivity to solvent loss, crystals of the three complexes were mounted in thin glass capillaries and cryopreserved at 100 K. Single crystals were introduced into the capillary suspended in a small volume of ether/DMF (solution used to grow the crystal saturated with ether). The data sets were collected on omega single-axis scans with 1-s per frame exposures at λ=0.82656 Å. The crystals were diffracting at a moderate resolution (2.3 Å) (see Supplementary Fig. 67) and showed degradation due to radiation damage, as seen from the intensities and resolution of the reflections after 266 (for 4·(BArF)8; see Supplementary Fig. 67), 220 (for C60⊂4·(BArF)8; see Supplementary Fig. 67) and 178 (C70⊂4·(BArF)8; see Supplementary Fig. 67) images. This poor density and fast degradation is attributed to the high symmetry, solvent loss and severe motions of the solvents (volatile ether) and counteranion molecules (BArF) in the large cavities of the crystal lattice. The three structures were solved by charge flipping method using the code Superflip57 and refined by the full matrix least-squares based of F2 using SHELX97 (ref. 58). Although the limited quality of the data (Supplementary Table 5) did not allow locating the counteranions and solvent molecules in the unit cell, the atomic positions of the atoms composing the cage and disordered C60 and C70 could be determined. For the same reasons, the atoms have been refined only isotropically. We provide, as additional data sets, preliminary CIF files extracted from partial refinement X-ray diffraction data, see Supplementary Data 3–5. For X-ray diffraction data of 4·(BArF)8, C60⊂4·(BArF)8 and C70⊂4·(BArF)8, see Supplementary Figs 65–69.

*Computational details*

All DFT calculations were performed using the ADF 2010 program. The molecular orbitals were expanded in an uncontracted set of Slater-type orbitals of double-ζ (DZ), and double-ζ (DZP) and triple-ζ (TZP) quality that contained diffuse functions and one set of polarization functions. The Frozen core approximation was used along the self-consistent field procedure. Scalar relativistic corrections have been included self consistently by using the zeroth order approximation. Energies and gradients were calculated by using the local density approximation (Slater exchange) with non-local corrections for exchange (Becke88) and correlation (Lee–Yang–Parr) included self consistently (that is, BLYP functional). Solvent effects (acetonitrile) were included through the use of COSMO approach. All structures were optimized using the QUILD program, which functions as a wrapper around the ADF program. QUILD uses improved geometry-optimization techniques, such as adapted delocalized coordinates and specially constructed model Hessians. When necessary, Cl− counteranions have been used instead of BArF− for reducing computational complexity. See the Supplementary Discussion 1 for a detailed description and corresponding references. For DFT structures of 4·(BArF)8 and its host–guest adducts, see Supplementary Figs 70–72 and Supplementary Data 1.

*Additional information*

How to cite this article: García-Simón, C. et al. Sponge-like molecular cage for purification of fullerenes. Nat. Commun. 5:5557 doi: 10.1038/ncomms6557 (2014).

## References

1 Giacalone, F. & Martín, N. Fullerene polymers: synthesis and properties. Chem. Rev. 106, 5136–5190 (2006).

2 Dennler, G., Scharber, M. C. & Brabec, C. J. Polymer-fullerene bulk-heterojunction solar cells. Adv. Mater. 21, 1323–1338 (2009).

3 Anthopoulos, T. D. et al. Air-stable n-channel organic transistors based on a soluble C84 fullerene derivative. Adv. Mater. 18, 1679–1684 (2006).

4 Norton, S. K., Conrad, D. H. & Kepley, C. L. J. Immunol. 182, 140–148 (2009).

5 Ryan, J. J. et al. Fullerene nanomaterials inhibit the allergic response. J. Immunol. 179, 665–672 (2007).

6 Parker, D. H. et al. Fullerenes and giant fullerenes: Synthesis, separation, and mass spectrometric characterization. Carbon N. Y. 30, 1167–1182 (1992).

7 Khemani, K. C., Prato, M. & Wudl, F. A simple Soxhlet chromatographic method for the isolation of pure fullerenes C60 and C70. J. Org. Chem. 57, 3254–3256 (1992).

8 Scrivens, W. A., Bedworth, P. V. & Tour, J. M. Purification of gram quantities of C60. A new inexpensive and facile method. J. Am. Chem. Soc. 114, 7917–7919 (1992).

9 Isaacs, L., Wehrsig, A. & Diederich, F. Improved Purification of C60 and Formation of σ- and π-Homoaromatic methano-bridged fullerenes by reaction with alkyl diazoacetates. Helv. Chim. Acta 76, 1231–1250 (1993).

10 Hirsch, A. & Brettreich, M. Fullerenes, Chemistry and Reactions Wiley-VCH (2005).

11 Yeretzian, C. et al. Partial separation of fullerenes by gradient sublimation. J. Phys. Chem. 97, 10097–10101 (1993).

12 Bhyrappa, P., Penicaud, A., Kawamoto, M. & Reed, C. A. Improved chromatographic separation and purification of C60 and C70 fullerenes. J. Chem. Soc. Chem. Commun. 13, 936–937 (1992).

13 Arias, F. et al. Kinetic effects in the electrochemistry of fullerene derivatives at very negative potentials. J. Am. Chem. Soc. 116, 6388–6394 (1994).

14 Xiao, J. & Meyerhoff, M. E. High-performance liquid chromatography of C60, C70, and higher fullerenes on tetraphenylporphyrin-silica stationary phases using strong mobile phase solvents. J. Chromatogr. A 715, 19–29 (1995).

15 Komatsu, N., Ohe, T. & Matsushige, K. A highly improved method for purification of fullerenes applicable to large-scale production. Carbon N. Y. 42, 163–167 (2004).

16 Canevet, D., Pérez, E. M. & Martín, N. Wraparound hosts for fullerenes: tailored macrocycles and cages. Angew. Chem. Int. Ed. 50, 9248–9259 (2011).

17 Tashiro, K. & Aida, T. Metalloporphyrin hosts for supramolecular chemistry of fullerenes. Chem. Soc. Rev. 36, 189–197 (2007).

18 Atwood, J. L., Koutsantonis, G. A. & Raston, C. L. Purification of C60 and C70 by selective complexation with calixarenes. Nature 368, 229–231 (1994).

19 Matsubara, H. et al. Supramolecular inclusion complexes of fullerenes using cyclotriveratrylene derivatives with aromatic pendants. Chem. Lett. 27, 923–924 (1998).

20 Kawase, T., Tanaka, K., Shiono, N., Seirai, Y. & Oda, M. Onion-type complexation based on carbon nanorings and a buckminsterfullerene. Angew. Chem. Int. Ed. 43, 1722–1724 (2004).

21 Tian, X.-H. & Chen, C.-F. Triptycene-derived calix[6]arenes: synthesis, structures, and their complexation with fullerenes C60 and C70. Chem. Eur. J. 16, 8072–8079 (2010).

22 Suzuki, K., Takao, K., Sato, S. & Fujita, M. Coronene nanophase within coordination spheres: increased solubility of C60. J. Am. Chem. Soc. 132, 2544–2545 (2010).

23 Haino, T., Fukunaga, C. & Fukazawa, Y. A new calix[5]arene-based container: selective extraction of higher fullerenes. Org. Lett. 8, 3545–3548 (2006).

24 Mahata, K., Frischmann, P. D. & Würthner, F. Giant electroactive M4L6 tetrahedral host self-assembled with Fe(II) vertices and perylene bisimide dye edges. J. Am. Chem. Soc. 135, 15656–15661 (2013).

25 Wang, M.-X., Zhang, X.-H. & Zheng, Q.-Y. Synthesis, structure, and [60]fullerene complexation properties of azacalix[m]arene[n]pyridines. Angew. Chem. Int. Ed. 43, 838–842 (2004).

26 Hu, S.-Z. & Chen, C.-F. Triptycene-derived oxacalixarene with expanded cavity: synthesis, structure and its complexation with fullerenes C60 and C70. Chem. Commun. 46, 4199–4201 (2010).

27 Pirondini, L. et al. Inclusion of methano[60]fullerene derivatives in cavitand-based coordination cages. Tetrahedron 62, 2008–2015 (2006).

28 Huerta, E. et al. Selective binding and easy separation of C70 by nanoscale self-assembled capsules. Angew. Chem. Int. Ed. 46, 202–205 (2007).

29 Isla, H. et al. A bis-exTTF macrocyclic receptor that associates C60 with micromolar affinity. J. Am. Chem. Soc. 132, 1772–1773 (2010).

30 Pérez, E. M., Sánchez, L., Fernández, G. & Martín, N. exTTF as a building block for fullerene receptors. Unexpected solvent-dependent positive homotropic cooperativity. J. Am. Chem. Soc. 128, 7172–7173 (2006).

31 Canevet, D. et al. Macrocyclic hosts for fullerenes: extreme changes in binding abilities with small structural variations. J. Am. Chem. Soc. 133, 3184–3190 (2011).

32 Huerta, E. et al. Tripodal exTTF-CTV hosts for fullerenes. J. Am. Chem. Soc. 132, 5351–5353 (2010).

33 Goeb, S. et al. A BPTTF-based self-assembled electron-donating triangle capable of C60 binding. Chem. Commun. 48, 3106–3108 (2012).

34 Gil-Ramírez, G. N. et al. A cyclic porphyrin trimer as a receptor for fullerenes. Org. Lett 12, 3544–3547 (2010).

35 Song, J., Aratani, N., Shinokubo, H. & Osuka, A. A porphyrin nanobarrel that encapsulates C60. J. Am. Chem. Soc. 132, 16356–16357 (2010).

36 Mulholland, A. R., Woodward, C. P. & Langford, S. J. Fullerene-templated synthesis of a cyclic porphyrin trimer using olefin metathesis. Chem. Commun. 47, 1494–1496 (2011).

37 Nobukuni, H. et al. Supramolecular structures and photoelectronic properties of the inclusion complex of a cyclic free-base porphyrin dimer and C60. Chem. Eur. J. 16, 11611–11623 (2010).

38 Schmittel, M., He, B. & Mal, P. Supramolecular multicomponent self-assembly of shape-adaptive nanoprisms: wrapping up C60 with three porphyrin units. Org. Lett. 10, 2513–2516 (2008).

39 Meng, W. et al. A self-assembled M8L6 cubic cage that selectively encapsulates large aromatic guests. Angew. Chem. Int. Ed. 50, 3479–3483 (2011).

40 Giguere, J.-B. & Morin, J.-F. New strapped porphyrins as hosts for fullerenes: synthesis and complexation study. Org. Biomol. Chem. 10, 1047–1051 (2012).

41 Hernández-Eguía, L. P. et al. Supramolecular inclusion complexes of two cyclic zinc bisporphyrins with C60 and C70: structural, thermodynamic, and photophysical characterization. Chem. Eur. J. 17, 14564–14577 (2011).

42 Sun, D., Tham, F. S., Reed, C. A., Chaker, L. & Boyd, P. D. W. Supramolecular fullerene-porphyrin chemistry. fullerene complexation by metalated ‘jaws porphyrin’ hosts. J. Am. Chem. Soc. 124, 6604–6612 (2002).

43 Nakamura, T., Ube, H., Miyake, R. & Shionoya, M. A C60-templated tetrameric porphyrin barrel complex via zinc-mediated self-assembly utilizing labile capping ligands. J. Am. Chem. Soc. 135, 18790–18793 (2013).

44 Boyd, P. D. W. & Reed, C. A. Fullerene−porphyrin constructs. Acc. Chem. Res. 38, 235–242 (2004).

45 Zhang, C., Wang, Q., Long, H. & Zhang, W. A highly C70 selective shape-persistent rectangular prism constructed through one-step alkyne metathesis. J. Am. Chem. Soc. 133, 20995–21001 (2011).

46 Inokuma, Y., Arai, T. & Fujita, M. Networked molecular cages as crystalline sponges for fullerenes and other guests. Nat. Chem. 2, 780–783 (2010).

47 Shoji, Y., Tashiro, K. & Aida, T. Selective extraction of higher fullerenes using cyclic dimers of zinc porphyrins. J. Am. Chem. Soc. 126, 6570–6571 (2004).

48 Li, M.-J., Huang, C.-H., Lai, C.-C. & Chiu, S.-H. Hemicarceplex formation with a cyclotriveratrylene-based molecular cage allows isolation of high-purity (≥99.0%) C70 directly from fullerene extracts. Org. Lett. 14, 6146–6149 (2012).

49 Kishi, N. et al. Facile catch and release of fullerenes using a photoresponsive molecular tube. J. Am. Chem. Soc. 135, 12976–12979 (2013).

50 Kishi, N., Akita, M. & Yoshizawa, M. Selective host–guest interactions of a transformable coordination capsule/tube with fullerenes. Angew. Chem. Int. Ed. 53, 3604–3607 (2014).

51 García-Simón, C. et al. Self-assembled tetragonal prismatic molecular cage highly selective for anionic π guests. Chem. Eur. J. 19, 1445–1456 (2013).

52 Juanhuix, J. et al. Developments in optics and performance at BL13-XALOC, the macromolecular crystallography beamline at the Alba Synchrotron. J. Synchrotron Rad. 21, 679–689 (2014).

53 Jiang, S. et al. Porous organic molecular solids by dynamic covalent scrambling. Nat. Commun. 2, 207 (2011).

54 Ribas, X., Costas, M., García-Simón, C., Company, A. & Gómez, L. Nanocápsulas moleculares para la separación selectiva de fullerenos. Patent P201430315 (2014).

55 Marcotte, N. & Taglietti, A. Transition-metal-based chemosensing ensembles: ATP sensing in physiological conditions. Supramol. Chem. 15, 617–625 (2003).

56 Ribas, X. et al. Stepwise construction of oligomeric 1,2-diselenolene platinum(IV) complexes. Angew. Chem. Int. Ed. 43, 4049–4052 (2004).

57 Palatinus, L. & Chapuis, G. SUPERFLIP—a computer program for the solution of crystal structures by charge flipping in arbitrary dimensions. J. Appl. Crystallogr. 40, 786–790 (2007).

58 Sheldrick, G. A short history of SHELX. Acta Crystallogr. A64, 112–122 (2008).

## Acknowledgements

This work was supported by grants from the European Research Council (Starting Grant Projects ERC-2011-StG-277801 and ERC-2009-StG-239910), the Spanish MICINN (CTQ2012-37420-C02-01/BQU, CTQ2012-32436, CTQ2011-23156/BQU, CTQ2011-25086/BQU, Consolider-Ingenio CSD2010-00065, INNPLANTA project INP-2011-0059-PCT-420000-ACT1, MAT2012-30994, a RyC contract to I.I., a JdC contract JCI-2012-14438 and CIG (FP7-PEOPLE-2013-CIG-630978) to S.O. and a PhD grant AP2010-2517 to M.G.B.) and the Generalitat de Catalunya (2009SGR637 and a PhD grant to C.G.S.). We thank Dr J.M. Luis and Professor M. Swart for fruitful discussions on DFT calculations, Dr C. Whiteoak for English grammar corrections, and Professor P. Ballester for providing us access to fluorescence spectroscopy measurements. X.R. and M.C. also thank ICREA-Acadèmia awards. Computational resources from Barcelona Supercomputing Center (Centro Nacional de Supercomputación) are acknowledged.

## Author information

*Affiliations*

Institut de Química Computacional i Catàlisi and Departament de Química, Universitat de Girona, Campus Montilivi, Girona, 17071, Catalonia, Spain

Cristina García-Simón, Marc Garcia-Borràs, Laura Gómez, Sílvia Osuna, Miquel Costas & Xavi Ribas

Serveis Tècnics de Recerca (STR), Universitat de Girona, Parc Cinetífic i Tecnològic, Girona, 17003, Catalonia, Spain

Laura Gómez

Servei de RMN and Departament de Química, Facultat de Ciències, Universitat Autònoma de Barcelona (UAB), Campus UAB, Bellaterra, 08193, Catalonia, Spain

Teodor Parella

ALBA Synchrotron, Cerdanyola del Vallès, Barcelona, 08290, Catalonia, Spain

Jordi Juanhuix

Institut Català de Nanociència i Nanotecnologia, ICN2, Campus UAB, Bellaterra, 08193, Catalonia, Spain

Inhar Imaz & Daniel Maspoch

Institució Catalana de Recerca i Estudis Avançats (ICREA), Pg. Lluís Companys 23, Barcelona, 08010, Catalonia, Spain

Daniel Maspoch

*Contributions*

C.G.-S. performed all the experimental work (cage synthesis and fullerene encapsulation/liberation experiments); M.G.-B. and S.O. performed the theoretical calculations; T.P. supervised the NMR studies; L.G. assisted in designing and performing the mass spectrometry studies; J.J., I.I. and D.M. performed and supervised all the crystallographic experiments at ALBA synchrotron; M.C. and X.R. designed and directed the project, and wrote the paper.

*Corresponding authors*

Correspondence to Miquel Costas or Xavi Ribas.

## Ethics declarations

*Competing interests*

The authors declare no competing financial interests.

## Supplementary information

*Supplementary Figures, Supplementary Tables, Supplementary Discussion*

Supplementary Figures 1-72, Supplementary Tables 1-5, Supplementary Discussion, Supplementary Methods and Supplementary References (PDF 5439 kb)

*Supplementary Data 1*

Optimized xyz cartesian coordinates for all DFT structures. (DOCX 129 kb)

*Supplementary Data 2*

CIF file for Clip_Me2ppPd. (CIF 22 kb)

*Supplementary Data 3*

CIF file for cage_4. (CIF 15 kb)

*Supplementary Data 4*

CIF file for C60_cage4. (CIF 20 kb)

*Supplementary Data 5*

CIF file for C70_cage4. (CIF 29 kb)

## Rights and permissions

*Reprints and Permissions*